N O T I C E

THIS DOCUMENT HAS BEEN REPRODUCED FROM MICROFICHE. ALTHOUGH IT IS RECOGNIZED THAT CERTAIN PORTIONS ARE ILLEGIBLE, IT IS BEING RELEASED IN THE INTEREST OF MAKING AVAILABLE AS MUCH INFORMATION AS POSSIBLE

(NASA-CR-168508) NUMERICAL SIMULATION OF THE INTERACTION OF THE PLASMA SHEET WITH THE LOBES OF THE EARTH'S MAGNETOTAIL (Alaska Univ., Fairbanks.) 46 p HC A03/MF A01 CSCL 04A H2/46

N82-16634

Unclas 07708

NUMERICAL SIMULATION OF THE INTERACTION OF THE PLASMA SHEET WITH THE LOBES OF THE EARTH'S MAGNETOTAIL

RECEIVED
NASA STI FACILITY
ACCESS DEPT.

by
Daniel W. Swift
Geophysical Institute
University of Alaska
Fairbanks, Alaska 99701

Abstract

Codes involving one and two spatial dimensions and three velocity dimensions are used to model the earth's magnetotail. It is shown that the magnetotail can become inflated as a consequence of low energy plasma convection toward the neutral plane. The two-dimensional code shows the development of small-scale turbulence. However, the growth of the turbulence appears limited, and does not lead to substantial dissipation. A one-dimensional model was used to simulate a particle population consisting of plasma sheet ions and cold lobe plasma. An applied convection electric field causes plasma sheet thinning and later expansion, consistent with observed substorm morphology. During the course of a simulated substorm the cold particles are heated and merge with the plasma sheet population. The magnetic field energy shows a slight increase, followed by a more rapid decrease as all of the cold particles are swept into the magnetotail. The code exhibits a conversion of both magnetic field energy and of energy supplied by the convection electric field into particle energy. The simulations suggest that much of the magnetotail substorm morphology may be a simple consequence of an increase, followed by a decrease, in the convection electric field, without the requirement of any magnetospheric size scale plasma instability or other disruptive processes. It is also concluded that the presence of the convection electric field and a continuing replenishment of low energy particles in the magnetotail lobes are both necessary for maintenance of the magnetotail.

1. Introduction.

Ever since the discovery of the neutral and plasma sheets in the earth's magnetotail considerable attention has been focused upon the relationships between the morphology of these features and the dynamics of auroral substorms. For a comprehensive review of this subject, see Akasofu (1979). It is generally accepted that (Akasofu, 1979; Fairfield et al., 1981) that the onset of a substorm, as determined from ground-based indicators, coincides with the thinning of the plasma sheet followed by a subsequent expansion. The substorm morphology of the magnetic field in the lobe does not seem to show as constant a pattern of increase or decrease (Akasofu, 1979). A southward turning of the field in the magnetotail is sometimes seen, which has been interpreted as a consequence of the formation of an x-type neutral line earthward of the point of observation (Hones, 1979). Others (Akasofu, 1979, and references contained therein) have interpreted the southward turning as simply the tilting of the magnetic field.

One intriguing feature of the earth's magnetotail is that it contains a large amount of free magnetic energy that could be converted to particle energy if the plasma sheet dynamics were to permit a relaxation to a more "dipolar" configuration. Schindler (1974) has suggested that the plasma sheet thinning during the growth phase of a substorm leads to an ion tearing mode instability which results in a release of magnetic energy. Birn (1980) has developed a numerical fluid model for the magnetotail. This model indicates stability if there is no viscous or resistive dissipation in the plasma; but a conversion of magnetic or kinetic energy does occur when the model contains dissipation.

Akasofu (1980a, b), on the other hand has identified a solar wind parameter, ε, involving the solar wind velocity and interplanetary magnetic

field, with the dimensions of energy flux, that shows a remarkable correlation with the magnetospheric substorm AE index. The fact that the ϵ and AE parameters have such a similar variation suggests that the substorm is externally driven, rather than the results of an instability internal to the magnetosphere (Swift, 1979).

For this reason, this paper adopts a very different approach to magnetotail dynamics by allowing energy input into the magnetotail by a convection electric field, and investigating processes that may lead to the formation of the highly stretched tail. The model also includes processes for energy exchange between the tail field and particles, so that processes investigated by Schindler (1974) and Birn (1980) can occur in the model to be described below. However, since a particle model will be used, there are no dissipation processes other than that allowed by the equations of motion of a charged particle in the electromagnetic field. Moreover, the model does not describe equilibrium processes or departures from equilibrium so the results are not easily compared to results of stability analysis.

The approach taken follows along some of the ideas expressed by Cowley (1980). He suggests that very low energy plasma, of solar wind or ionospheric origin finds its way into the lobes of the earth's magnetotail, whence it is swept into the neutral sheet by the convection electric field. In the nonadiabatic encounter with the neutral sheet, the plasma is accelerated earthward and heated (Swift, 1977), thus converting cold lobe plasma into a population with the characteristics of the plasma sheet. These ideas are given further support by the recent observations with the Hawkeye satellite. Anderson and Eastman (private communication) have made measurements of the plasma line cutoff in the lobes of the magnetotail which indicate plasma densities in the range of 0.1 to 1.2 cm^{-3}. Since the presence of these

particles is not indicated by the particle detectors, their energy must be below detection threshold, hence they are likely of ionospheric origin.

In summary, the calculations will be directed toward answering the question of whether the main characteristics of the observed tail morphology can be understood in terms of a process of polar wind, or magnetosheath ions being swept from the lobes into the neutral sheet region by a convection electric field. To this end, we shall consider both one and two-dimensional models in a plane continuing the magnetic field, which is assumed to be the magnetospheric noon-midnight meridian plane. The two-dimensional code can be used to investigate possible development of turbulence and O- and X-type neutral lines (Stern, 1979; Vasyliunas, 1980). The one-dimensional code can be used, because of the much greater economies of operation, to observe the system over a much longer time span in relation to the particle gyroperiod. It turns out that turbulence does develop in the two-dimensional simulation, but that the turbulence does not seem to affect the large-scale morphology. As a result, the one-dimensional model appears to offer a good representation of the total dynamics.

In the next section, the model will be described, along with a brief description of the numerical procedures. The following section will present the results of the calculations, and the final section will present a comparison between the model results and the observed substorm morphology of the earth's magnetotail.

2. Calculation Procedure.

2.1 Formulation of the Model.

The basic code used is a nonradiative electromagnetic code similar to that described by Nielson and Lewis (1976) in which we neglect all electrostatic interactions among particles and assume uniformity in the y-

direction. Electrostatic interactions are neglected because we also assume the existence of a highly mobile population of cold electrons which is capable of shorting out potentials developed along field lines. Possible electrostatic effects will be described in the concluding section. We further assume that the magnetic field is confined to the x-z planes. This and the assumption of y-symmetry implies that the only allowed currents are in the y-direction. This also means that currents carried by $E \times B$ and field-aligned motion of ions and electrons cancel and that the x and z-components of the current due to gyrational motion and polarization drifts of the ions average to zero. The assumption of y-symmetry also precludes instabilities excited by cross-tail current flow (Huba et al., 1978; Tanaka et al., 1981) which may lead to anomalous resistivity and electron heating.

These assumptions make it possible to describe the entire system in terms of the y-component of the vector potential of which the only source is the y-component of the ion motion. We therefore consider the following system of equations for the ion motion.

$$\frac{dv_x}{dt} = \frac{e}{mc} v_y B_z \qquad (1a$$

$$\frac{dv_y}{dt} = \frac{e}{m} E_y + \frac{e}{mc} (v_z B_x - v_x B_z) \qquad (1b$$

$$\frac{dv_z}{dt} = - \frac{e}{mc} v_y B_x \qquad (1c$$

where E_y is the electric field, which includes both a convection electic field and the solenoidal field due to the time rate of change of $\vec{B}$. The magnetic field $\vec{B}$ is expressed in terms of the vector potential

$$(B_x, 0, B_z) = (-\frac{\partial}{\partial z} A_y, 0, \frac{\partial}{\partial x} A_y) \qquad (2$$

where A_y is the y-component of the vector potential, which satisfies the equation

$$\nabla^2 A_y(\vec{r}) = -4\pi e \sum_k S(\vec{r} - \vec{r}_k)\, v_{yk} \qquad (3$$

where the sum is over all particles present in the system, and $\vec{r}_k$ is the instantaneous position of the particle, and v_{yk} its velocity along y. $S(\vec{r})$ is a normalized density function which differs from a simple δ-function because in a numerical simulation the charge must be assigned to neighboring grid points. $\vec{r}_k$ is found by integrating

$$\frac{d\vec{r}_k}{dt} = \vec{v}_k \qquad (4$$

with $\vec{v}$ calculated from (1). In (1) the field terms are actually evaluated according to

$$\vec{B}(\vec{r}_k) = \int \vec{B}(\vec{r})\, S(\vec{r} - \vec{r}_k)\, dxdz \qquad (5$$

At this stage it is useful to introduce dimensionless units in order that the system can be scaled to run with economically practical particle numbers, and distance and time scales. To this end, we introduce dimensionless position and time coordinates.

$$\vec{\xi} = \vec{r}/\rho \qquad (6a$$

$$\tau = \omega t \qquad (6b$$

where ρ and ω are a nominal gyroradius and gyrofrequency. The dimensionless velocity becomes

$$\vec{v} = \frac{d\vec{\xi}}{d\tau} = \vec{v}/(\omega\rho)$$

The equations of motion (1) become

$$\frac{d\vec{v}}{d\tau} = (\vec{\varepsilon} + \vec{v} \times \vec{\Omega})/\omega \qquad (7$$

where $\vec{\Omega} = e\vec{B}/(mc)$, and $\vec{\varepsilon}$ is the electric field acceleration $\vec{\varepsilon}=e\vec{E}/(m\omega\rho)$. A dimensionless vector potential $\tilde{A}_y$ is introduced

$$\tilde{A}_y = A_y \frac{e}{mc\omega\rho} \qquad (8$$

such that

$$\nabla_\xi \times (\tilde{A}_y \vec{1}_y) = \vec{\Omega}/\omega \qquad (9$$

with these substitutions, the equation for $\tilde{A}_y$ is given by

$$\nabla_\xi^2 \tilde{A}_y = -\alpha v_y \tilde{n} \qquad (10$$

where α is the coupling constant

$$\alpha = \frac{4\pi e^2}{mc^2} \qquad (11$$

and

$$v_y\tilde{n} = \rho^2 \sum_k S(\vec{\xi} - \vec{\xi}_k)\, v_{yk} \qquad (12$$

The problem is scaled for computation by selecting the number of particles and the size of the domain, and then selecting an appropriate value for the coupling constant. We can also, without loss of generality, set $\omega = 1$, and for the sake of convenience make the variable replacements $\vec{\xi} \to \vec{x}$, $\vec{v} \to \vec{v}$, $\tilde{A}_y \to A_y$. It will also be useful to split the electric field acceleration into the solenoidal, $\varepsilon_s = \partial A_y/\partial t$, and the convective term ε_c which represents the dawn-to-dusk convection electric field.

The particle and field equations in the new <u>dimensionless</u>, simulation units, now read

$$\frac{dv_x}{dt} = \Omega_z v_y \qquad (13a$$

$$\frac{dv_z}{dt} = -\Omega_x v_y \qquad (13b$$

$$\frac{dP_y}{dt} = \varepsilon_c \qquad (13c$$

where the field variables at the position of the kth particle are computed according to the prescription given in (5). P_y is the canonical momentum and is used to calculate v_y.

$$v_{yk} = P_{yk} - \int A_y(\vec{r})\, S(\vec{r}-\vec{r}_k)\, d^2x \qquad (14$$

Use of the canonical momentum makes it possible to avoid the explicit appearance of the destabilizing $\partial A_y/\partial t$ term in the equation for v_y (Nielson and Lewis, 1976). The equation for the vector potential, A_y, can be written in the form

$$\nabla^2 A_y(\vec{r}) = -\alpha(P(\vec{r}) + n(\vec{r})A_y(\vec{r})) \qquad (15$$

where

$$P(\vec{r}) = \sum_k P_{yk}\, S\,(\vec{r}-\vec{r}_k) \qquad (16a$$

and

$$n(\vec{r}) = \sum_k S\,(\vec{r}-\vec{r}_k) \qquad (16b$$

The particle gyrofrequency is calculated from

$$(\Omega_x,\ 0,\ \Omega_z) = (\frac{\partial A_y}{\partial z},\ 0,\ -\frac{\partial A_y}{\partial x}) \qquad (17$$

In addition to the field generated by the local particle currents, we will wish to include a constant, uniform magnetic field in the z-direction. The earth's dipole field, and possibly the interplanetary magnetic field, could contribute a z-component, but not necessarily uniform field. However making provision for a nonuniform, asymptotic z-component, would greatly complicate the calculation. Hence, A_y in (15) will include an additive term, $A_y \rightarrow A_y + \Omega_0 x$, which gives rise to a uniform magnetic field in the z-direction of intensity Ω_0.

Before describing the numerical procedure, it will be useful to make note of important relations expressed in the simulation units of (13)-(17). Multiplying the equations (13a, b) by v_x and v_z respectively, and the equation

$$\frac{dv_y}{dt} = \varepsilon - v_x\Omega_z + v_z\Omega_x$$

by v_y and summing over all the particles, the energy conservation law is obtained

$$\frac{d}{dt}\left[\sum_k \frac{1}{2} v_k^2 + \frac{1}{2\alpha}\int \Omega^2\, dxdz\right] = \frac{1}{\alpha}\int \varepsilon\, \vec{1}_y \times \vec{\Omega} \cdot d\vec{s} \qquad (18$$

where the integral over $\vec{ds}$ is an integral over a boundary surface. From this expression we identify $\Omega^2/2\alpha$ as the magnetic energy density and $\varepsilon\vec{1}_y \times \vec{\Omega}/\alpha$ as the Poynting flux. The E × B drift is $\vec{u}_E = \varepsilon_c \vec{1}_y \times \vec{\Omega}/\Omega^2$. Another important parameter is the Alfvèn velocity, V_a, which given by the expression,

$$V_a^2 = \Omega^2/(\alpha n) \qquad (19$$

where n is computed from (16b).

2.2 Two-dimensional Numerical Procedures.

The integration of the particle equations of motion (13a, b) and the non-dimensional version (4) is accomplished by the standard leap-frog scheme, with the x- and z-components of the velocities and positions being advanced a half time-step apart. The value of P_y in (13c) is advanced following the calculation of A_y; thus v_y, which is calculated from (14), is at the same time-step of the position coordinates, but a half time-step removed from the

(v_x, v_y) variables. Therefore, the particle pushing algorithm is second order accurate. The integration of (13c) is only first order accurate, but since P_y changes nearly linearly with time this introduces little error.

An iteration scheme is used to solve (14) is similar to that used by Lin (1978), namely

$$\nabla^2 A_y^{\ell+1} - \alpha\bar{n}\, A_y^{\ell+1} = -\alpha P + \alpha(n-\bar{n})\, A_y^{\ell} \qquad (20$$

where the superscript ℓ refers to the iteration number. The $\ell=0$ iteration is the last iteration of the previous time-step. $\bar{n}$ is a constant parameter. If $\bar{n}$ is too small, the iteration is unstable, and if $\bar{n}$ is too large, the convergence will be slow. This slow convergence is due to the fact that the Green's function for the operator on the right hand side is $G = \exp(-R\sqrt{\alpha\bar{n}})/R$, where $R=|\vec{r}-\vec{r}\,'|$. Thus, if there is a change in the current at $\vec{r}\,'$, the effect of this change will propagate only a distance $(\alpha\bar{n})^{-1/2}$ each iteration. Large values of $\bar{n}$ require either a large number of iterations between time-steps, or very short time-steps in comparison to the time scale of the simulation, in order that changes in one part of the domain might propagate across the entire domain. Nielson and Lewis (1976) suggest $\bar{n} = \frac{1}{2}(n_{max} + n_{min})$.

The equation for $A_y^{\ell+1}$ is a constant-coefficient, Helmholtz equation of the type

$$(\nabla^2 - k^2)\, A(\vec{r}) = -p(\vec{r}) \qquad (21$$

In solving this equation, we can neglect the $\Omega_0 x$ term of the constant background field, because in the numerical procedure the term $\alpha n \Omega_0 x$ is incorporated into the αP term on the right-hand side of (20). This makes it

possible to solve (21) subject to periodic boundary conditions in x for a domain of length L.

Equation (21) is solved using Fourier transform methods. The details of the method which allow the imposition of boundary conditions at $z = 0$ and $z = L$ is given in the appendix. Essentially, the boundary conditions are that the x-component of the magnetic field, averaged over x at $z = 0$ and L be equal and opposite and that the similarly averaged boundary values of the vector potential be constant.

The source terms in the equation of A_y, shown in (16) are computed by a standard four-point area-weighting scheme in which the contribution of the current is distributed at the four surrounding grid points. Momentum conservation therefore requires that the interpolation of the fields as indicated in (5) be the usual bilinear four-point Lagrangian scheme. Therefore, each particle contribution to the current is represented as values at the four grid points defining the cell which contains the particle. No other smoothing of the particle density such as the Gaussian weighting, is used, because this would introduce inconsistencies in the boundary conditions.

The particle boundary conditions are assumed periodic in x. That is if $x > L$, the replacement $x \to x-L$ is used, and v_x and v_z are unchanged. A similar replacement is used if $x < 0$. However, because of the background magnetic field, Ω_0, the value of P_y must be changed by an amount $\pm\Omega_0 L$ when a particle crosses the $x = 0$, L boundaries. It is this change in P_y on crossing the $x = 0$, L boundaries that would give rise to problems if a Gaussian charge weighting scheme were used. If a particle were located at $x = L - \delta$, part of the charge would appear at the $x = 0$ grid points, with a totally inappropriate value of P_y attached, which would give rise to spurious boundary currents. When the particle crosses the $z = 0$, L boundaries, which is an unusual event

because of the inward convection, it is reinserted in the domain at the same boundary, on the same guiding center, but with the velocity reinitialized to the E × B drift.

2.3 One-Dimensional Numerical Procedures.

In the one-dimensional problem all field variables depend only on the z-coordinate, except for the vector potential which is written

$$A_y(x, z) = a(z) + \Omega_z x \tag{22}$$

where Ω_z is constant. The field equation for a is therefore

$$\frac{d^2a}{dz^2} = -\alpha \sum_k (P_{yk} - a(z) - \Omega_z x_k)\, S(\vec{r} - \vec{r}_k) \tag{23}$$

Upon integrating (23) over x from 0 to L and dividing by L, we obtain

$$\frac{d^2a}{dz^2} - \frac{\alpha}{L} n(z)a = -\frac{\alpha}{L} \sum_k (P_{yk} - \Omega_z x_k) S(z - z_k) \tag{24}$$

where

$$n(z) = \sum_k S(z-z_k) \tag{25}$$

since the only x-dependence in (24) occurs with P_{yk}, we can define a new variable

$$\tilde{P}_{yk} = P_{yk} - \Omega_z x_k \tag{26}$$

and (13c) is replaced by

$$\frac{d\tilde{p}_{yk}}{dt} = \varepsilon_c - \Omega_z v_{xk} \tag{27}$$

where v_{xk} is advanced by (13a), and it is no longer necessary to keep track of x_k for each particle. The field equation is now given by

$$\frac{d^2a}{dz^2} - \alpha_1 n(z)a = -\alpha_1 \tilde{p}(z) \tag{28}$$

where

$$\tilde{p} = \sum_k \tilde{p}_{yk} S(z - z_k) \tag{29}$$

and α_1 is the one-dimensional charge coupling constant. $\tilde{p}$ and n are calculated using a linear weighting scheme and the field values at the particles are calculated from grid points by linear interpolation.

No iteration is necessary in solving (28) because it can be solved efficiently for variable n(z) by using the finite difference approximation to the derivative, and using the tri-diagonal algorithm (Roache, 1976) for calculating a(z) at the grid points.

In the problem at hand, we can assume reflection symmetry about the z = 0 plane. It is therefore sufficient to consider only the domain from the center of the neutral sheet outward into the lobe of the magnetotail. Since the x-component of the magnetic field vanishes, one boundary condition is that $\partial a/\partial z = 0$ at z = 0, the assumed position of the neutral sheet. At the other end of the domain, we wish the value of a to be constant, so that in the absence of a convection electric field, the Poynting flux vanishes. However, if we have a region between the neutral sheet and the end of the domain in which there are no particles, that is, where the source term for (28)

vanishes, the value of $Q_x = da/dz$ will be constant, so it is necessary to calculate the solution only where $n(z)$ is assured of being nonzero.

Let the domain be divided into two regions, $0 < z < L$ and $L < z < L + D$, and let n be zero in the latter region. We therefore need to integrate (28) only in the region $0 < z < L$, with the boundary condition at $z = L$, $a + D\partial a/\partial z = 0$. This mixed boundary condition is easily incorporated into the finite difference, tri-diagonal algorithm (Roache, 1976). In this case, the total magnetic energy is given by

$$E_m = \frac{1}{2\alpha_1}\left[\int_0^L Q_x^2\, dz + DQ_x^2(L) + (L + D)Q_z^2\right] \qquad (30$$

Reflecting boundary conditions must be used in the particles at $z = 0$. This means that a particle which finds itself at $z < 0$, the replacement $z \to -z$ and $v_z \to -v_z$ is made. The other phase space variables are unchanged. These boundary conditions follow from the assumption of reflection symmetry. When a particle from the north passes through the symmetry plane, it is replaced by a particle from the south side in which the z component of velocity is reversed. This coupled with the fact that $Q_x = 0$, makes the $z = 0$ boundary absolutely energy conserving. Particles which exceed $z = L$ are simply reinserted inside the domain, and the velocities are reinitialized to the $E \times B$ drift velocity. Although this particle boundary condition is not energy conserving, very few particles cross the $z = L$ boundary.

3. Results of Calculations.

3.1 Two-Dimensional Model Results.

The two-dimensional calculations seek to examine the question of how the earth's magnetotail and neutral sheet might be inflated and respond to

changing external conditions, such as the imposed convection electric field. The calculations also seek to explore whether turbulence would develop, and whether it would lead to the formation of X- and O-type neutral lines.

As a working hypothesis it is assumed that a convection electric field is present in a region accessed by cold particles of ionospheric or magnetosheath origin. Panel a of Figure 1 shows the initial magnetic field configuration. This was generated as a contour plot of the vector potential. The magnetospheric z-axis is upward, and the x-axis, earthward direction, increases to the right. In the region where the magnetic field is uniform the x- and z-components of $\vec{\Omega}$, as it appears in (13a, b) is set ot 0.5. The source of the x-component of the field is a current sheet, which is held constant in time, but has small random spatial perturbation.

Contours of constant current density are exhibited in panel a of Figure 2. It was necessary to introduce this current because the interation procedure outlined in (2) requires a starting vector potential consistent with the initial particle distribution. This current sheet was assumed in order to introduce a kink in the magnetic field and the perturbation in the current sheet to excite any plasma instabilities that might develop. It will become apparent that this ad-hoc current will be a small fraction of the total particle current. Some field-line curvature is necessary, in order that the $E \times B$ drift not be everywhere inertial. It is only in the region where the $E \times B$ drift is non-inertial that ions will move relative to electrons.

The planes shown in Figure 1 are defined by 129×129 grid points, which are loaded with 4×10^4 particles in a band 129×89 grid points centered on the neutral sheet. The average density is $4 \times 10^4/(128 \times 88) = 3.55$ particles per cell. This is the initial value of n in (16b). The initial particle velocities are all set to the local $E \times B$ drift velocity, such that they

initially contribute nothing to the current. The charge coupling parameter, α, in (15) is set to $\alpha = 0.0655$, which results in the asymptotic Alfvén speed of $V_a = 3.040$. The convection electric field is 7.07, so that the asymptotic x and v-components of the E × B drift velocity are $\vec{u}_E = (7.07, 0, \pm 7.07)$, with the z-components converging on the neutral plane. The initial E × B drift energy of the plasma is 2.179×10^6, and the initial energy in the magnetic field is 6.02×10^4. Hence, in this model the E × B drift energy far exceeds the magnetic energy, for the boundary condition that the vector potential is clamped on the z = 0 and z = L boundaries. The time-step for this model was $\Delta t = 0.025$, and eight iterations were used each time-step to calculate A_y.

Figure 1b shows the magnetic field lines a short while later. The significant change is that the kink in the field lines is sharper. Figure 2b shows the current density contours are also much narrower. The fixed current shown in Figure 2a is unchanged, but the largest contribution to the current comes from the particles drifting into the neutral plane. The current sheet appears thinner because the number of contours between maximum and minimum is constant, independent of the difference between these values.

Figures 1c and 2c show the field lines and current contours somewhat later. The current has bifurcated, and this is reflected in the development of shock structures on either end of the neutral plane, which develop because the flow toward the neutral plane exceeds the phase velocity of a magnetosonic wave. This super-magnetosonic flow is by virtue of the assumed cold particle distribution and very small magnetic field intensity. It would not be seen in an established plasma sheet and magnetotail in which particle thermal energies and magnetic field intensitites are much higher. The thickness of the shock is the order of resolution of the grid mesh. At the time corresponding Figures 1d and 2d, all of the particles have been swept into the shock region,

and the external field begins to increase. The asymptotic field lines appear somewhat curved in Figure 1d because not quite enough iterations have been taken to communicate the information from the edge of the current sheet to the boundary of the domain. The feature of main interest in Figure 2d is the development of multiple current sheets and the expansion of the current carrying region.

Figure 1e shows the continued increase of the external field and the continued thickening of the current carrying region. A satellite traversing the plasma sheet would observe multiple reversals in the x-component of the field. Figure 2e shows the development of current filaments and x-dependent structure. Plots of the z-component of the magnetic field at the original neutral plane show considerable short wavelength fluctuation.

Finally, Figures 1f and 2f, at the end of the run show the development of turbulence in the plasma sheet region with some closed magnetic islands. The run could not be carried on much longer because the current sheets would have expanded to the edge of the domain. The external x-component of the field has increased to 3.25, a factor of 6.5 over the x-component at the beginning of the run. This clearly indicates that the action of a convection electric field on a cold particle population is capable of significantly increasing the lobe field.

Figure 3 shows plots of the magnetic, kinetic and total energies during the run. The total energy began to increase at a more rapid rate only after all of the cold particles were swept into the current sheet and the external field began to increase. Since the convection electric field was held constant, the value of Poynting flux at the boundaries would increase in proportion to the boundary field. Also, it appears that the width of the current channel has a nearly steady increase.

An important question is the fate of the turbulence seen in Figures 1f and 2f. The fact that the current sheet has successively broken into many smaller current sheets, and the fact that the irregularities have the same size scale on the x- and z-directions suggests that the turbulent cells will not coalesce to form large scale structures of the type that would be identified with the development of a single or a few X-type neutral lines in the magnetosphere, or the development of the topology that emerged from the fluid calculations of Birn (1980). This conclusion is based on another run similar to that shown in Figures 1 and 2, except that the convection electric field was only half the value. This made it possible to carry the run on for a longer period of time. Turbulence also developed at about t = 15 into the run, and it was tracked until t = 20 at the end of the run. During the period the turbulence on the original center of the current sheet was observed to go through a cycle of growth, decay and regrowth, suggesting that the level of turbulence is stable. In this latter run, the diameter of the turbulent cells was the same as the width of the current sheets; however, the scale size and amplitudes were somewhat smaller than the scale size and amplitudes of the runs shown in Figures 1-3, with the stronger convection field. These results seem to be consistent with the results of fluid model simulations of Matthaeus and Montgomery (1981) of a sheet pinch which exhibited the development of small scale MHD turbulence. The turbulence did not lead to any enhanced energy dissipation.

The most serious limitation of these runs is that the time span was not much longer than the characteristic ion gyroperiod. The possible consequences of this limitation will be discussed after the one-dimensional results are presented. Another point that should be kept in mind is that the magnetic field is very weak, so that the flows are super-magnetosonic.

The model does seem to indicate a process for the inflation of the earth's magnetotail by a convection electric field. The model also suggests that, aside from low-level turbulence, a one-dimensional, z-dependent model of the neutral/plasma sheet may provide an adequate description.

3.2. One-Dimensional Model

An advantage of the one-dimensional model is that it is economically feasible to follow a system for a very large number of time-steps. Moreover, since the fields are calculated implicitly, no iteration is necessary, and action-at-a-distance is possible. This makes it easy to follow rapidly propagating Alfvèn waves.

The total model domain will extend from $z = 0$ to $z = 256$, but the particles will be confined to $0 < z < L = 128$. As explained in Section 2.3, the $z = 0$ boundary is assumed to be the center axis of the current sheet with the boundary condition $\Omega_x = 0$. The vector potential is held fixed at $z = 256$. The model uses 8192 particles, divided initially into two populations. There is a hot population consistency of 2048 particles loaded into the region $0 < 32$. The particles are randomly distributed in z; their speeds are uniformly, randomly, distributed in the range $0 < v < 10\sqrt{2}$; and the velocity directions are uniformly, randomly, distributed on the surface of a sphere. This population represents the plasma sheet. The charge coupling constant, α_1 of (28), was set to 3.9×10^{-3} in order that this population would support an asymptotic magnetic field of $\Omega_x = 5$. The other population consists of 6144, zero velocity particles which are spatially distributed according to

$$n_c(z) \begin{cases} = zn_0/32 & z < 32 \\ = n_0 & 32 < z < 112 \\ = n_0(127 - z)/15 & 112 < z < 127 \\ = 0 & z > 127 \end{cases} \qquad (31$$

where $n_0 = 59.4$. The z-component of the magnetic field is $\Omega_z = 1$, so with $\Omega = 5.1$, and a particle density of n_0, the Alfvén velocity is $V_\alpha = 10.6$. Two separate runs were made with the one-dimensional model. One assuming a convection electric field, ϵ_c, that increases linearly from zero to 10 at $t = 2\pi$ and thereafter remains constant. The other is a nearly energy-conserving run with $\epsilon_c = 0$.

The results of the run with the convection electric field are displayed in Figures 4, 5, and 6, which show the particle number density, particle energy density and x-component of the magnetic field respectively at various stages of the run. The magnetic field lines are displayed in the contour plots of $a(z) + \Omega_z x$ in Figure 7, while Figure 8 shows a time history of the magnetic, kinetic and total energy. Figure 9 shows a plot of the final particle energy spectrum.

The initial x-component of the magnetic field was computed self-consistently with the plasma sheet particles, so if there were no z-component of the magnetic field and no electric field, the field and particle population would be in equilibrium. The stresses due to the addition of a z-component of the magnetic field will cause an acceleration of the plasma in the x-direction, while the y-directed electric field will cause a particle drift toward the neutral plane. It can be seen that the cold portion contributes very little to the current. At t = 6 and 12, the effect of the convection electric field compressing the particle near the neutral plane can be seen.

This would be viewed as a thinning of the plasma sheet, a signature of substorm onset. The waves in the magnetic field profile are due to Alfvén waves propagating outward from the plasma sheet, which are generated by initial transients due to the fact that the initial particle and field distributions were not chosen completely self-consistently. During this growth phase Figure 8 indicates a slow increase in magnetic energy and a much more significant increase in kinetic energy.

The middle portion of the run, from t = 30 to t = 70, saw an expansion of the plasma sheet, and a leveling off of the magnetic energy increase, but a continuing and accelerating increase in plasma energy. Figures 4 and 5 show a merging of the cold and plasma sheet populations at about t = 50. In contrast to the plasma sheet expansion; Figures 6 and 7 show a continuing decrease in the thickness of the magnetic neutral sheet during this middle period. Also, the magnetic field profiles indicate the existence of standing, shock-like features near the neutral sheet.

The final phase of the run from t = 70 to 110, shows a continuing expansion of the plasma sheet, but now also shows a substantial thickening of the neutral sheet. At this time, all of the ionospheric plasma has been swept into the neutral sheet and heated. The most significant feature of this later phase is the continuing increase in plasma energy and the comparatively rapid decay of magnetic energy. The magnetic field energy decays despite the continuing presence of the convection electric field. This indicates that maintenance of the tail field requires a continuing supply of cold particles to be swept into the neutral sheet region.

Finally, Figure 9 shows the particle energy spectrum at the final stage of the run. Also shown for purpose of comparison is the energy spectrum

$$f(E)dE = 4.40\ E^{1/2} e^{-E/\theta}\ dE$$

where $\theta = 164$, corresponding to a three-dimensional Maxwellian distribution of velocities that has the same average energy as the simulation energy spectrum. The most significant features is that the simulation spectrum is much more peaked than a thermal distribution. The spectrum is also characterized by a long tail, containing relatively few particles that decay quite slowly, with the highest energy particles at 1819.

Figure 10 shows magnetic, kinetic and total energy for a run which had the same initial phase space distribution of particles, but in which there was no convection electric field present. The result is that magnetic energy immediately begins to decay with the energy going into kinetic energy of the particles. This is an energy-conserving run, so the total energy should remain constant. The degree to which the total energy remains constant is a measure of the accuracy of the code. During the run, there was a 3.7% increase in total energy. The plots of density, energy density, and magnetic field during the early phase of the run showed little noteworthy differences between the run and the run with the convection electric field present, except that toward $t = 40$, the run with the convection electric field present began to show a thicker plasma sheet. Comparison of the two runs suggests that the presence of a convection electric field is necessary to keep the tail field from collapsing. During the field collapse the solenoidal electric field was the same order as the applied convection electric field in the previous example, $\varepsilon_s = 10$.

There are significant differences between the one and two-dimensional runs. The two-dimensional run exhibited strong shock formation. This is attributed to the fact that in the two-dimensional run the flow was super-

magnetosonic. The other major difference was the absorption of particle energy in the one-dimensional simulation. This is due to the fact that the one-dimensional simulation contained an energetic thermal population and that the one-dimensional run had a duration of several gyroperiods such that the cold population became heated and thermalized. Another difference is that in the one-dimensional simulation, the E × B drift energy increases by a factor of 26 between the asymptotic regions and the neutral sheet, while in the two-dimensional simulation, there is only a factor of two increase in E × B drift energy. Moreover, in the two-dimensional run when the particles encounter shocks in which there is a significant increase in the magnetic field, the E × B drift energy shows a decrease.

4. Discussion and Conclusion

The purpose of this paper has been to use one- and two-dimensional particle codes to model the formation and dynamics of the earth's magnetotail. The two-dimensional model was used to explore a process for the inflation of the earth's magnetic field into a configuration like the magnetotail. The process assumed the presence of cold particles and a convection electric field and an initial kink in the magnetic field caused by the assumed presence of a sheet current. The simulation showed that the cold particles drifting into the region of the current sheet would expand the current sheet and eventually increase the magnitude of the external field.

A question of interest is whether an arbitrarily small perturbation in an otherwise uniform field would give rise to the inflation exhibited in Figure 1. The firehose instability (Hasegawa, 1975) provides useful insight. The convection electric field may be transformed away by going to an inertial frame moving at $u = cE_y/B_z$. The result is particle streaming

parallel to the magnetic field at $v_{\parallel} = cE_yB_x/(BB_z)$. Particles originating from opposite sides of the current sheet will stream in opposite directions, resulting in interpenetrating ion beams. If one assigns a parallel kinetic temperature to this distribution of $\theta_{\parallel} = \frac{1}{2} m v_{\parallel}^2$, then the criterion for the firehose instability says the kinks will grow when

$$8\pi n\, \theta_{\parallel}/B^2 > 2$$

or

$$\frac{c^2}{V_a^2} \frac{E_y^2}{B^2} \tan^2\psi > 2 \qquad (32$$

where ψ is the angle of the asymptotic field lines make with the z-axis. For $\psi = 45^o$, $E = 1$ mV/m and $n = 1$ cm^{-3}, (32) is equivalent to $B < 5.7\gamma$.

Equation (32) can also be written in terms of the change in B_x across the current sheet, and it puts a lower limit on the size of a perturbation, given n, B_z and E_y. Equation (32), when ψ is expressed in terms of B_x shows that there is a minimum perturbation, below which perturbations will not likely grow. These runs however indicate that a magnetotail configuration like those presently observed could evolve from a very weak field through a series of repeated injections of cold particles to build up a plasma sheet population which supports its extended magnetotail lobes.

The other question addressed by the two-dimensional model is whether instabilities in the current sheet would likely develop which would lead to the formation of X- and O- type neutral lines. The indications from the model runs is that fine-scale turbulence does develop and in one model it does lead to the formation of closed flux lines, but it does not seem to lead to the large scale x-dependence that would be identified with the formation of X- and O-type neutral lines in the magnetosphere. These conclusions must remain

tentative until more extensive runs can be made. The code was run under conditions of super-magnetosonic convective flow, which might exist in only limited regions of the plasma sheet. It should also be run for longer time periods. Such runs must await extensive revision to the program to increase its efficiency.

The program also assumed a constant magnetic flux through the upper and lower boundaries of the simulation domain. This does not take account of the fact that as the magnetosphere is inflated, more and more field lines are pulled out into the tail. This could change the magnetic flux through the top and bottom boundaries in a localized region represented by the simulation domain. A sufficient decrease in the flux might permit the formation of large-scale magnetic islands.

The one-dimensional model also assumed a constant z-component of the magnetic field, and also x-independence of all quantities. In other respects it was more realistic, in that the initial magnetic field was supported by an initial distribution of hot particles, and that the convective flow velocities were less than the Alfvén speed. Moreover, the system was followed for a large number of ion gyroperiods. A substorm was modelled by applying an external convection electric field and assuming the existence of a population of cold particles external to the plasma sheet population, representing particles of ionospheric origin in the lobes of the magnetotail.

The plots of the energy density of the run shown in Figure 5, reproduce the well-documented thinning and re-expansion of the plasma sheet. This thinning is attributed to the inward $E \times B$ drift of plasma sheet particles. This occurs whether or not a convection electric field is applied, because in the absence of a convection electric field, an induction electric field develops due to the collapse of the magnetic field. This induction electric

field also causes an inward E × B drift. The subsequent expansion is a result of more energetic particles streaming outward from the neutral plane. If the field-aligned component of the particle velocity is large enough, the z-component of its motion can exceed the inward component of the E × B drift, resulting in plasma sheet expansion.

There also appears to be a thinning of the magnetic neutral sheet followed by a subsequent thickening, which lags considerably behind the thinning and thickening of the plasma sheet. However, an observer stationed at one position with respect to the neutral plane would observe no clear trend in the variation of the magnetic field. The thinning would only show up as a more rapid reversal of the x-component of the magnetic field on traversing the neutral sheet. The thickening of the magnetic neutral sheet occurred after all of the cold particles had been swept into the plasma sheet and thermalized. The thickening process also accompanied a decrease in magnetic energy.

The decrease in magnetic energy at this time, in spite of the continuing presence of the convection electric field, suggests that a necessary condition for the maintenance of the tail field is the continued influx of cold particles from the lobes of the magnetotail. This in turn implies the necessity of replenishing the lobe field lines with particles of magnetosheath origin. Figure 10, which shows the variation of magnetic and particle energy for a run in which there was no convection electric field, shows the immediate onset of magnetic energy decrease. This suggests that the presence of a convection electric field is also a necessary condition for the maintenance of the tail field. The fact that when both cold particles and the convection electric field are present, the magnetic field energy remains constant or increases, suggests that a necessary and sufficient condition for the

existence of the magnetotail is the combined presence of the convection electric field and cold particle populations in the magnetotail lobes.

The results of the simulation allow us to tentatively identify the manifestations of a substorm in the magnetotail as simply a consequence of an increase in the convection electric field. It appears that a quasi-steady-state field and particle configuration can be maintained with a modest convection electric field and a continuous supply of ionospheric or magnetosheath particles to the lobes. A temporary increase in the convection electric field would bring about the thinning and re-expansion of the plasma sheet. There would be enhanced dissipation which would heat the plasma sheet population, but since there would also be other low energy particles in the process of being heated a satellite observer would not necessarily observe an increase in plasma temperature. The lobe magnetic field could increase or decrease depending on the availability of low energy particles. The substorm decrease in magnetic energy observed by Fairfield et al. (1981) could follow a consequence of the depletion of the cold lobe particles. These processes take place without the occurrence of any large-scale plasma instability.

The simulations suggested that the plasma sheet would continue to thicken whether or not a convection electric field is present, so there would be no way for the plasma sheet to return to its original configuration. Therefore, the complete cycle requires some process for the removal of plasma sheet particles. In the magnetosphere this can be accomplished through the convection of plasma sheet particles into the inner portions of the magnetosphere to become part of the ring current belt.

Another important result is the fact that convection electric field or magnetic field energy can be readily converted into particle energy; and as predicted by Roederer (1977), this can occur in the absence of any magnetic

region associated with a neutral line. Fluid codes, on the other hand, require the special introduction of viscosity or resistivity in order to effect such a conversion (Birn, 1980; Matthaeus and Montgomery, 1980). The ready conversion of energy in ordered plasma flow to thermal energy is possible because as Swift (1977) and Wagner (1979) have shown, ions interact non-adiabatically with the magnetic neutral sheet region where the ordered flow energy is converted into gyrational motion. This has the same effect as dissipation.

The simulation time scale can be scaled to the magnetospheric time scale by the particle gyrofrequency. In the one-dimensional model, we have assumed a five-to-one ratio between the lobe and neutral sheet field strengths, which is not unreasonable. If we assume a lobe field of 15γ, then a simulation time duration of 110 corresponds to a time of 383 sec if H^+ ions are assumed and 6130 sec for O^+. The time assuming H^+ populations is shorter than actual substorm times. The time duration of the simulation could easily be increased by populating a greater portion of the magnetotail lobes with cold particles. One effect of a longer run would likely be a broader spectrum of particle energies than indicated in Figure 9.

Distances can be scaled on particle gyroradius. A 1 keV ion is a 15γ field has a gyroradius of 300 km. A numerical simulation velocity is 10, giving a simulation gyroradius of 2 grid units. The intial half-thickness of the simulation plasma sheet is 32 grid units, which would correspond to 4800 km, somewhat less than observed plasma sheet thicknesses. An electric field of 10 units gives an $E \times B$ drift velocity of 10 units in the neutral plane, which corresponds to a velocity of 436 km/sec (1 keV) in magnetospheric units. In a 3γ field, this corresponds to a convection electric field of 1.3 mV/m. The equivalent number density of cold plasma can be obtained by

comparison of Alfvèn velocities. In a magnetic field of 5 gyrofrequency units and a density of 59.4, the Alfvèn velocity is $V_a = 10.38$, which corresponds to a magnetospheric Alfvèn velocity of 458 km/sec. A number density of 0.53 cm^{-3} gives this Alfvèn velocity in a 15γ field. This number density is well within the range reported by Anderson and Eastman (private communication).

Finally, we wish to assess possible effects of electrostatic fields arising from charge separation. Electrons and ions will follow different trajectories in regions where the magnetic field is non-uniform. As mentioned previously, we anticipatethat highly mobile electrons will be effective in maintaining charge neutrality along magnetic field lines. However, in regions where the magnetic field curvature is large, ions will stream perpendicular to field lines through strongly magnetized electrons. This could excite the modified two-stream instability (McBride et al., 1972). This instability can give rise to substantial electrostatic potential which would substantially change ion trajectories. This is a subject currently under investigation with a purely electrostatic code involving both electron and ion dynamics. This process offers the intriguing prospect of generating large potential differences across field lines. Such potentials may play a role in accelerating auroral electrons.

Another possible interaction involving electrostatic fields is the lower hybrid drift wave. This mode is excited by currents in the y-direction, but plasma sheet density gradients act to destabilize the mode so that excitation occurs at lower current thresholds. Huba et al. (1977, 1978) point out that such instabilities can give rise to anomalous resistivity and enhanced dissipation, perhaps sufficient to allow ion tearing mode instability. However, the calculations presented here and individual particle calculations done elsewhere (Swift, 1977, Wagner et al., 1979) have shown that the cross-

tail electric field can result in the transfer of energy to gyrational motion of ions. This can have the same effect as dissipative term in the fluid equations, namely transfer of energy from ordered motion to internal degrees of freedom. Therefore, even if the model calculations reported here permitted excitation of the lower hybrid drift instability, it is not certain that this would significantly effect the calculations. Moreover, Schindler and Birn (1978) have pointed out that when $B_z > 0$ everywhere, and the tail field is in equilibrium with pressure gradients that it is stable against all modes. Although the conditions on the model do not involve equilibrium, the Schindler-Birn theorem suggests that the models used here might be stable against the tearing mode.

Acknowledgement. This work was supported by the Atmospheric Science Section of the National Science Foundation under Grant ATM-79 23614 and by the National Aeronautics and Space Administration under Grant NSG-7625.

Appendix

Details of Numerical Procedures to Solve Equation (21).

The method of solution is similar to that described by Dycek and Dawson (1978). Equation (21) is Fourier transformed in x so that

$$A(x, z) = \sum_m A(m, z)\, e^{2\pi i m x/L}$$

where A(m, z) satisfies

$$\left(\frac{\partial^2}{\partial z^2} - \frac{4}{\Delta x^2} \sin^2 \frac{\pi m}{N} - k^2\right) A(m, z) = -p(m, z) \qquad \text{(A1}$$

where N+1 is the number of grid points on $[0 \leq x \leq L]$ and Δx is the distance between grid points.

We wish to solve (A1) subject to the boundary condition that the magnetic field must be asymptotically uniform. In order to impose this condition, we write (Decyk and Dawson, 1979)

$$A(m, z) = a(m, z) + \tilde{A}(m, z) \qquad \text{(A2}$$

where $\tilde{A}(m, z)$ is the periodic solution, calculated from

$$\tilde{A}(m, z) = \sum_n \tilde{A}(m, n)\, e^{2\pi i n z/L}$$

where $\tilde{A}(m, n)$ is given by

$$\tilde{A}(m, n) = p(m, n) \left[4\, \frac{\sin^2(\pi m/N)}{\Delta x^2} + 4\, \frac{\sin^2(\pi n/N)}{\Delta z^2} + k^2 \right]^{-1} \qquad \text{(A3}$$

where $p(m, n)$ is the double Fourier transform of $p(\vec{r})$ in (21), and Δz is the distance between grid points along the z-axis.

The other term in (A2) satisfies the homogeneous part of (A1). Using the finite difference approximations to the second partial derivative, it can be shown that

$$a(j, m) = A_m r^j + B_m r^{-j} \qquad \text{(A4}$$

where j is the index denoting the grid point number along the z-axis, and $r = \eta + \sqrt{\eta^2+1}$, where η is given by

$$\eta = 1 + 2\frac{\Delta x^2}{\Delta z^2}\sin^2(\pi m/N) + \frac{1}{2}k^2\Delta z^2 \qquad \text{(A5}$$

For $m > 1$, the coefficients A_m and B_m are determined by the condition that $A(m, j)$ where $j = z/\Delta z$, join smoothly onto solutions which vary as r_e^j at $j = 0$ and r_e^{-j} at $j = N$, where $r_e = \eta_e + \sqrt{\eta_e^2+1}$, where η_e is calculated as in (A5), but with k^2 set equal to zero. For the $m = 0$ solution to (A1), we impose the boundary conditions that

$$A'(0, 0) = -A'(0, N) \qquad \text{(A6a}$$

and

$$\frac{1}{2}(A(0, 0) + A(0, N) = A_0 \qquad \text{(A6b}$$

where the primes denote the finite difference approximation to the derivative with respect to z. Equation (A6a) requires that the x-componentd of the magnetic field at $z = 0$ and L be equal and of opposite sign, while (A6b) requires that the value of $\partial A/\partial z$ averaged over the boundary vanish. In the

absence of the convection electric field, (A6b) specifies that there be no net Poynting flux across the boundary.

References

Akasofu, S.-I., Chapter 6 in Physics of Magnetospheric Substorms, D. Reidel, Dordrecht-Holland, 1979.

Akasofu, S.-I., The solar wind-magnetospheric energy coupling and magnetospheric disturbances, Planet. Space Sci., 28, 495, 1980a.

Akasofu, S.-I., Study of individual geomagnetic storms in terms of the solar wind, Planet. Space Sci., 28, 933, 1980b.

Birn, J., Computer studies of the dynamic evolution of the geomagnetic tail, J. Geophys. Res., 85, 1214, 1980.

Cowley, S.W.H., Plasma populations in a simple open model magnetosphere, Space Sci. Rev., 26, 217, 1980.

Decyk, V.K. and J.M. Dawson, Computer model for bounded plasma, J. Computational Physics, 30, 407, 1979.

Fairfield, D.H., R.P. Lepping, E.W. Hones, Jr., S.J. Bame, and J.R. Asbridge, Simultaneous measurements of magnetotail dynamics of IMP Spacecraft, J. Geophys. Res., 86, 1396, 1981.

Hasegawa, A., Plasma Instabilities and Nonlinear Effects, Springer-Verlag, New York, 1975.

Hones, E.W. Jr., Transient phenomena in the magnetotail and their relation to substorms, Space Sci. Rev., 23, 393, 1979.

Huba, J.D., N.T. Gladd and K. Papadopoulos, Lower-hybrid-drift wave turbulence in the distant magnetotail, J. Geophys. Res., 83, 5217, 1978.

Huba, J.D., N.T. Gladd and K. Papadopoulos, The lower-hybrid-drift instability as a source of anomalous resistivity for magnetic field line reconnection, Geophys. Res. Lett., 4, 125, 1977.

Lin, A.T., Nonlinear evolution of Alfvèn and double tearing instabilities, Phys. Fluids, 21, 1026, 1978.

McBride, J.B., E. Ott, J.P. Boris and J.H. Orens, Theory and simulation of turbulent heating by the modified two-stream instability, Phys. Fluids, 15, 2367, 1972.

Matthaeus, W.H. and D. Montgomery, Nonlinear evolution of the sheet pinch, J. Plasma Physics, 25, 11, 1981.

Nielsen, C.W. and H.R. Lewis, Particle-code model in the nonradiative limit in Methods of Computational Physics, 16, Academic Press, New York, 1976.

Roache, P.J., Computational Fluid Dynamics, Hermosa Publishers, Albuquerque (1976).

Roederer, J.G., Global problems in magnetospheric plasma physics and prospects for their solutions, Space Sci. Rev., 21, 23, 1977.

Schindler, K., A theory of the substorm mechanism, J. Geophys. Res., 79, 2803, 1974.

Schindler, K. and J. Birn, Magnetospheric Physics, Physics Reports, 47, 111, 1978.

Stern, D.P., The role of O-type neutral lines in magnetic merging and solar flares, J. Geophys. Res., 84, 63, 1979.

Swift, D.W., The effect of the neutral sheet on magnetospheric plasma, J. Geophys. Res., 82, 1288, 1977.

Tanaka, M., T. Sato and T. Kamimura, A computer simulation on microinstabilities and anomalous resistivity near the magnetic neutral sheet, to be published in J. Geophys. Res., 1981.

Vasyliunas, V.M., Upper limit on the electric field along a magnetic O line, J. Geophys. Res., 85, 4616, 1980.

Wagner, J.S., J.R. Kan and S.-I. Akasofu, Particle dynamics in the plasma sheet, J. Geophys. Res., 84, 891, 1979.

ORIGINAL PAGE IS
OF POOR QUALITY

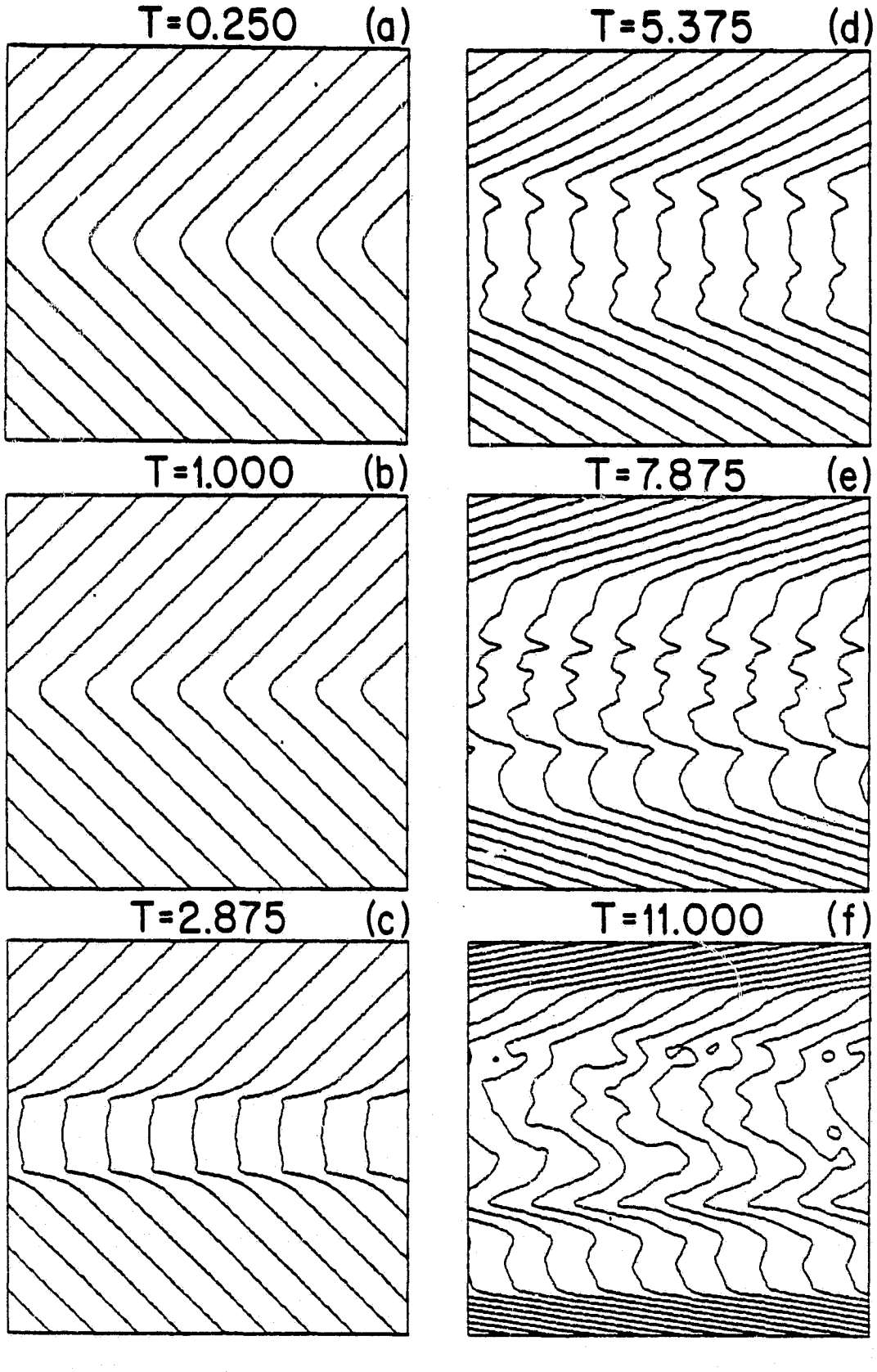

Figure 1. Contour plots of the magnetic vector potential showing the magnetic field lines during various stages of a run exhibiting the development of a plasma sheet. Earthward is toward the right and the vertical is the magnetospheric z-axis.

ORIGINAL PAGE IS
OF POOR QUALITY

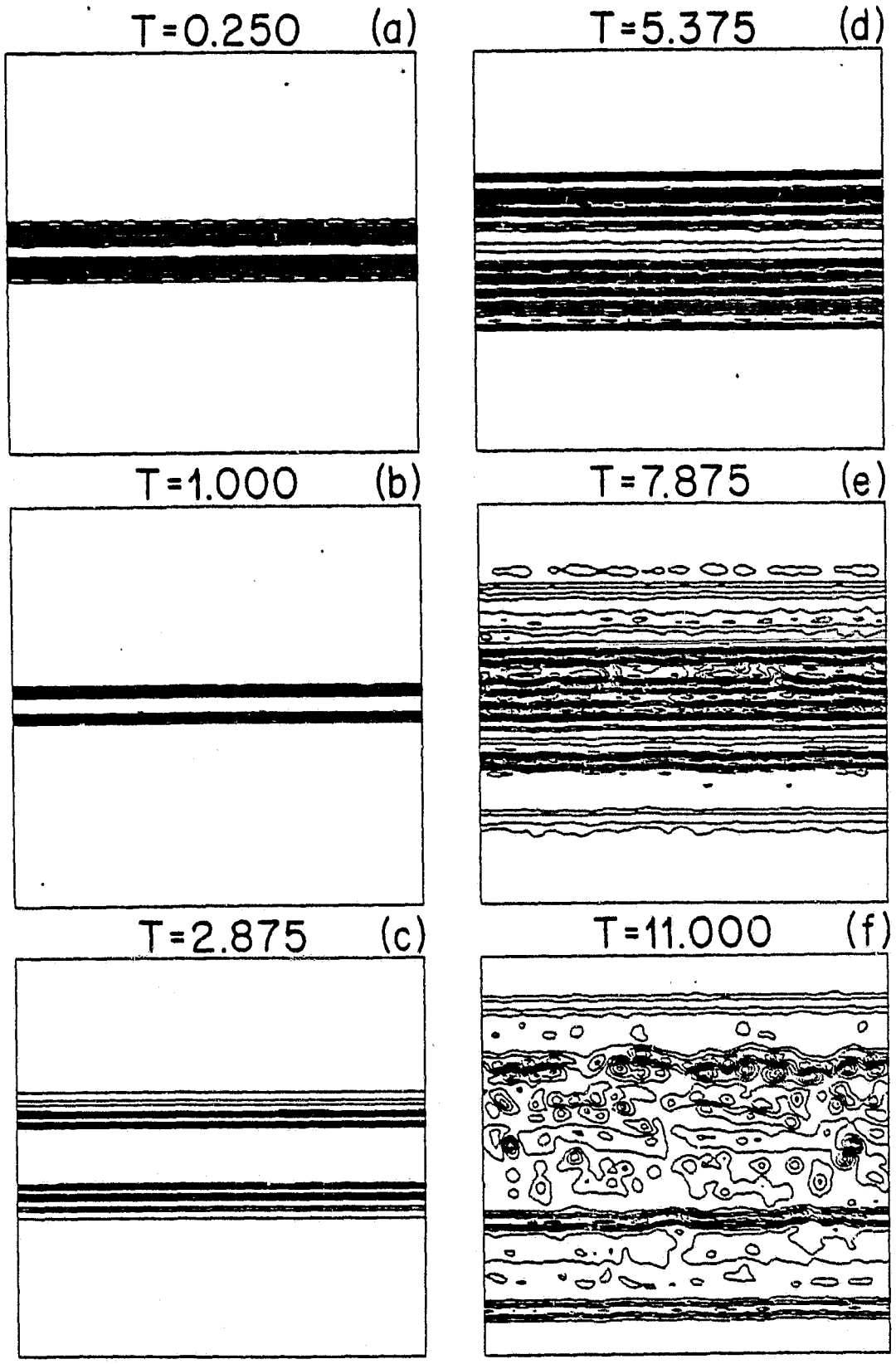

Figure 2. Contours of constant current density for the same model shown in Figure 1. The current is perpendicular to the page. There are 11 contour intervals between the minimum and maximum.

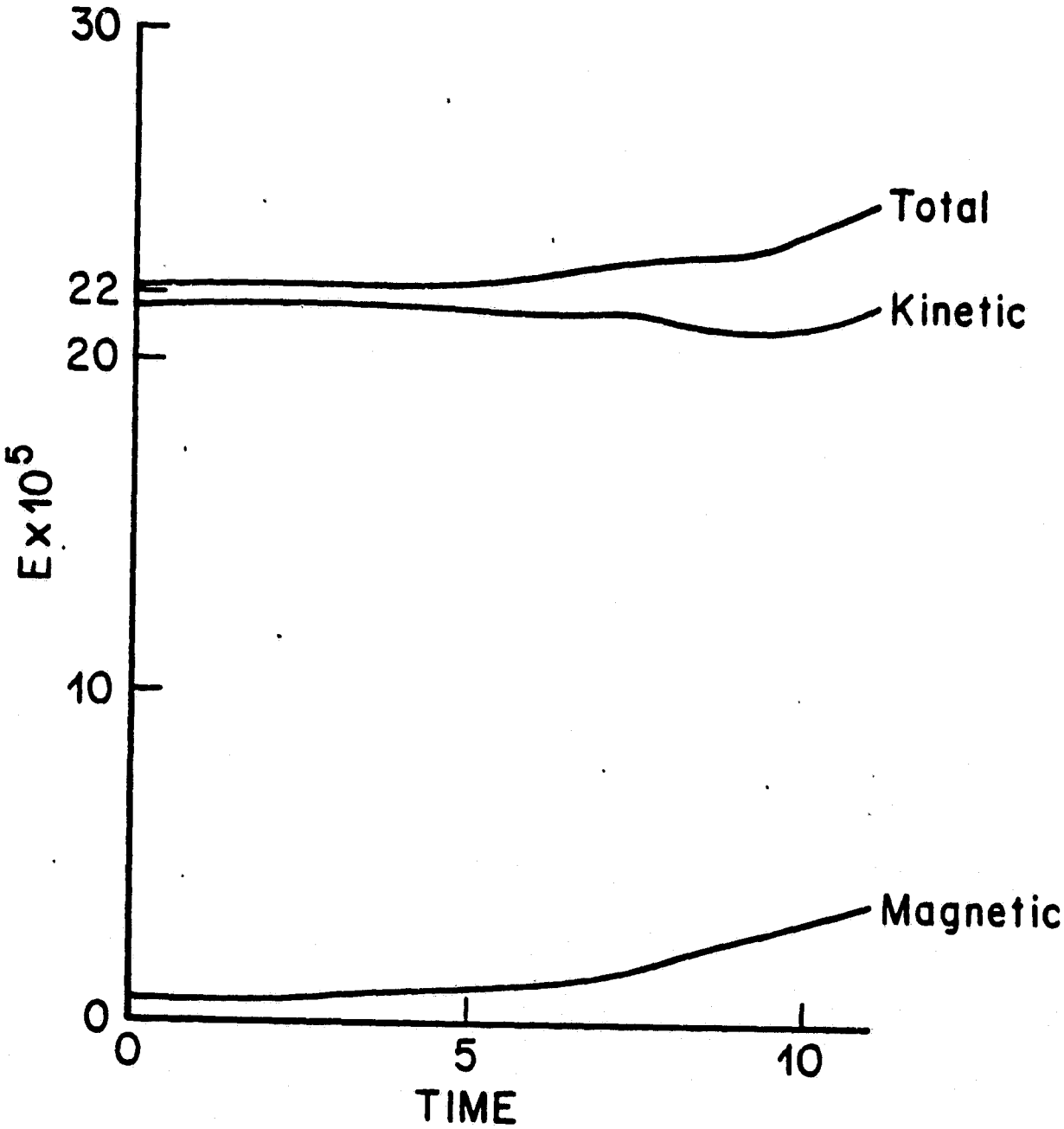

Figure 3. A plot showing the magnetic, kinetic and total energy during the run shown in Figures 1 and 2. The energy is in units of $0.5v^2$ where v is the particle velocity in simulation units.

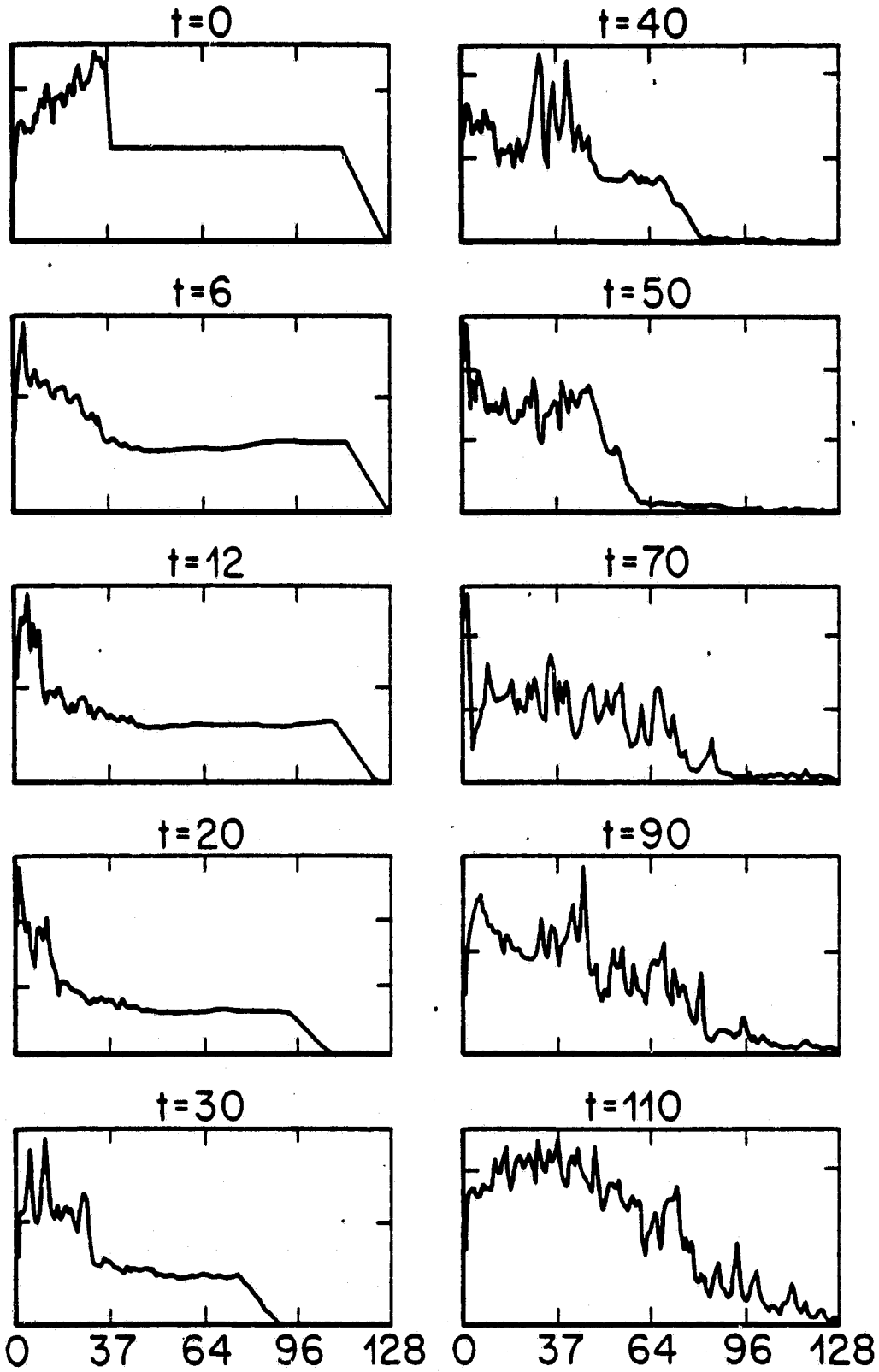

Figure 4. Number density profiles as a function of the distance from the symmetry plane, expressed in grid units. The density is expressed in particles per grid unit. The tic marks show densities in units of 100.

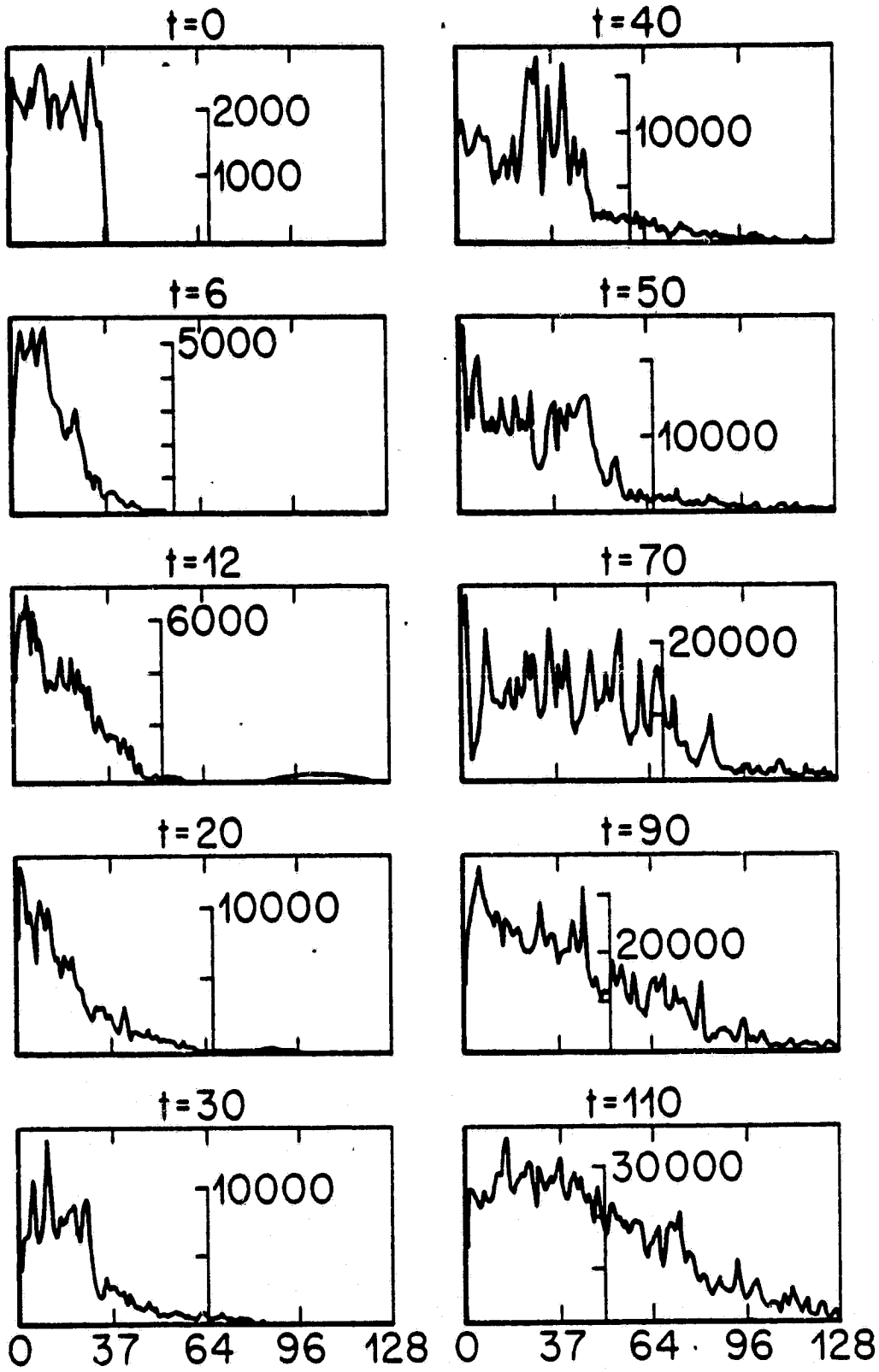

Figure 5. Particle energy density profiles for the run shown in Figure 4. Comparisons between the two figures make it possible to distinguish between regions occupied by cold and energetic particles.

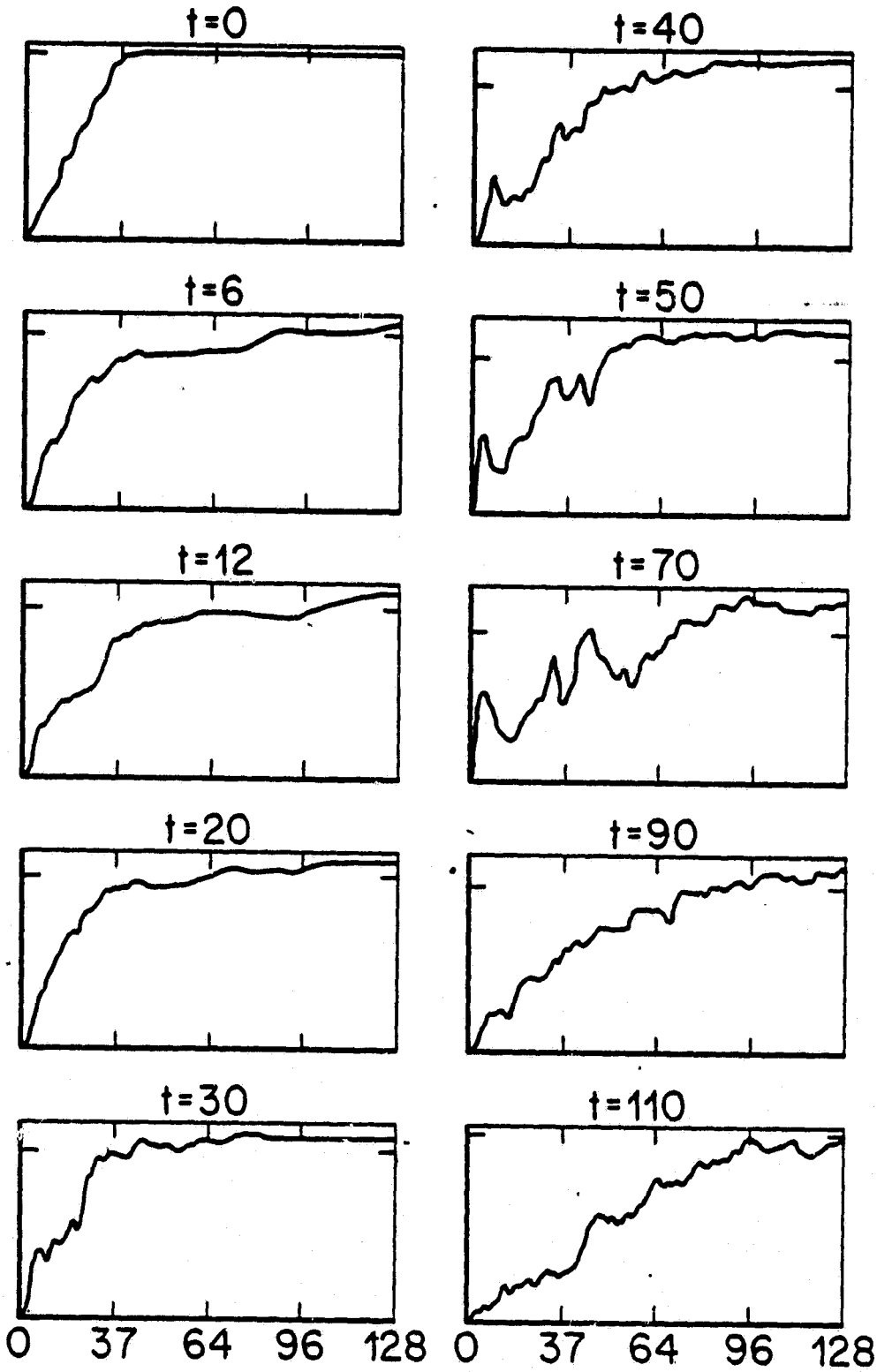

Figure 6. Profiles of the x-component of the magnetic field for the run depicted in Figures 4 and 5. The tic marks show a field strength of 5 in simulation units.

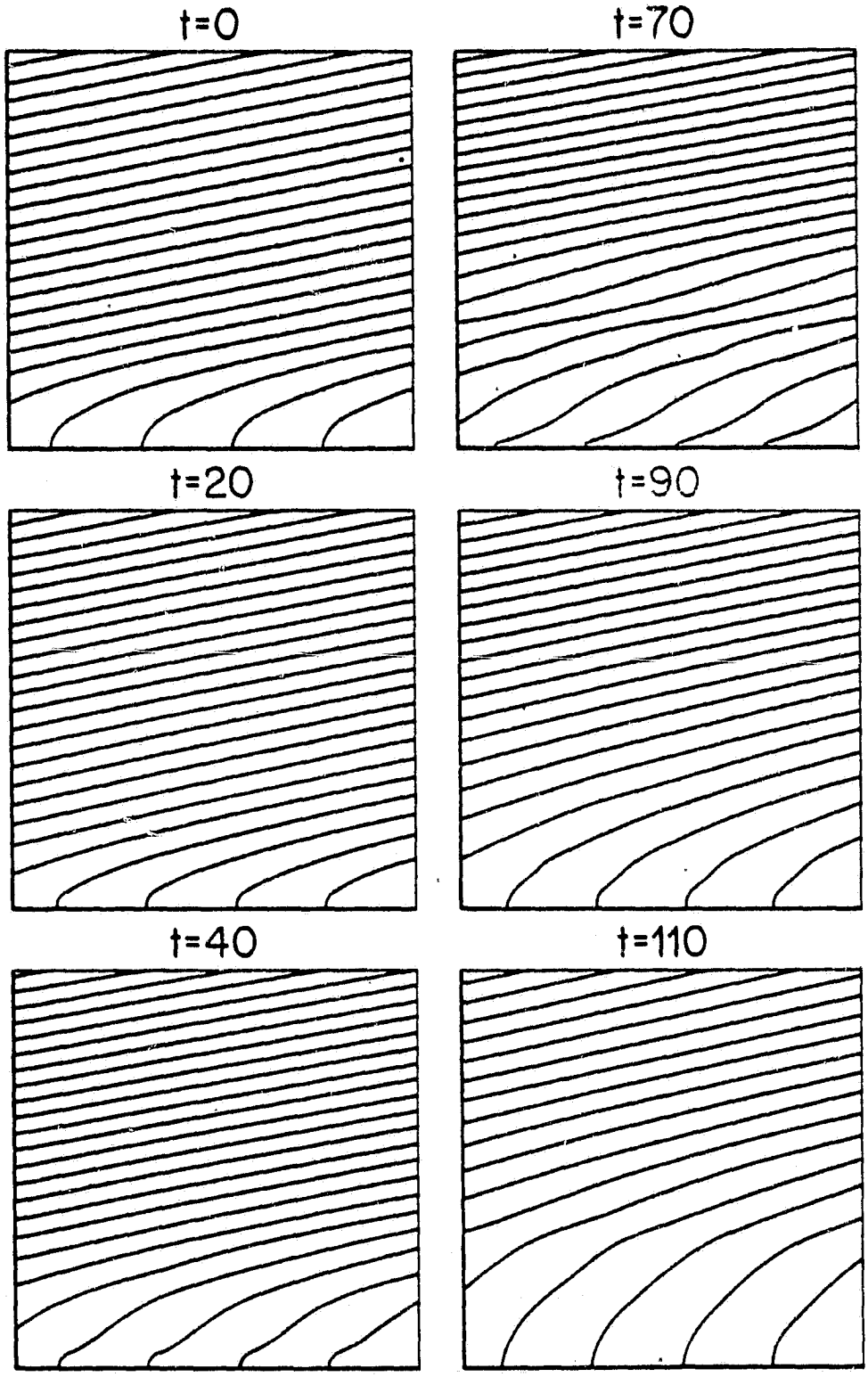

Figure 7. Contour plots of the vector potential $A_y = a(z) + \Omega_z x$ showing magnetic field lines for some of the profiles shown in Figure 6. The bottom edge is at the neutral plane, while the top edge is at $z = 128$.

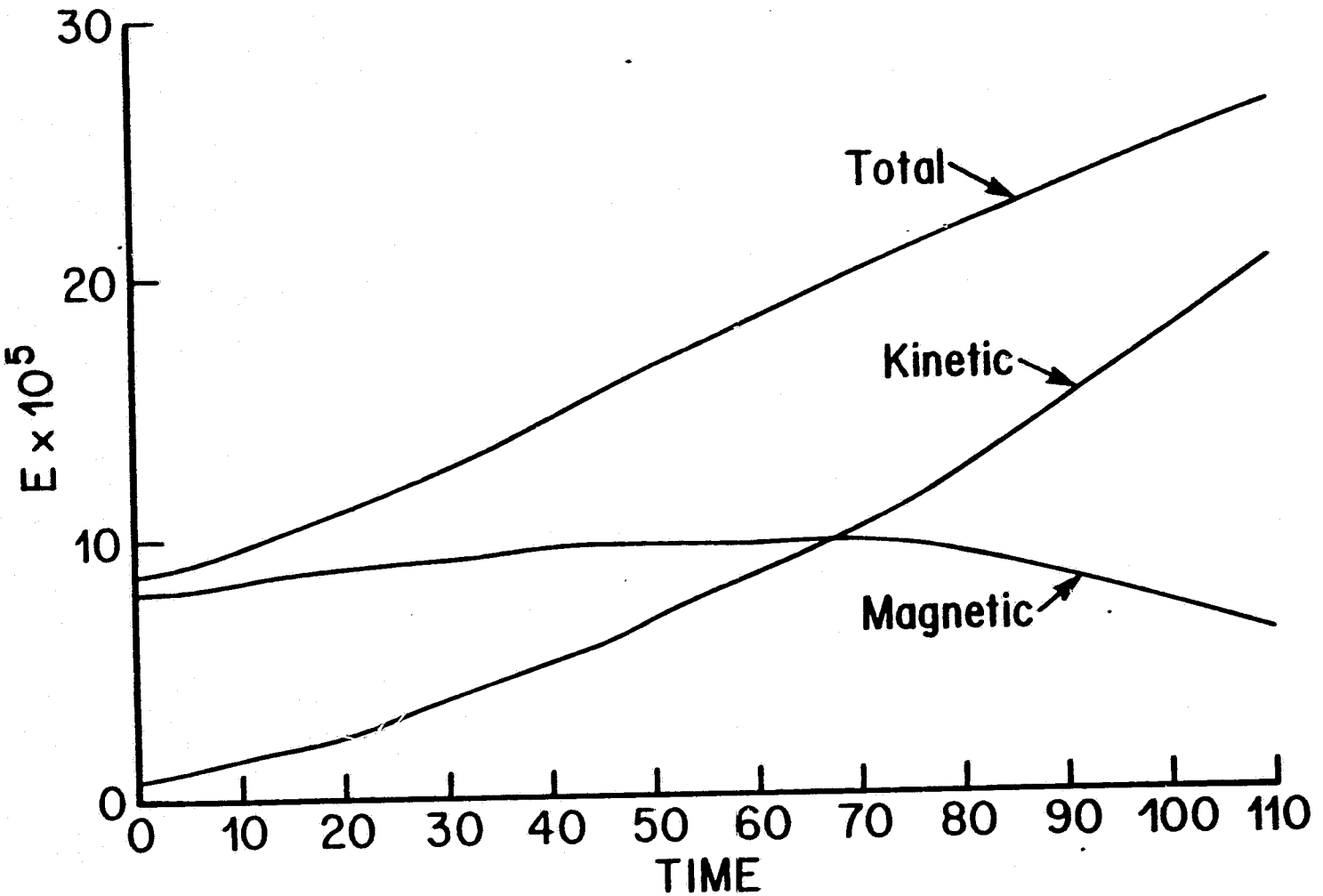

Figure 8. A plot showing the time variation of kinetic magnetic and total energy during the run depicted in Figures 4-7. Energy is in units of $\frac{1}{2}v^2$.

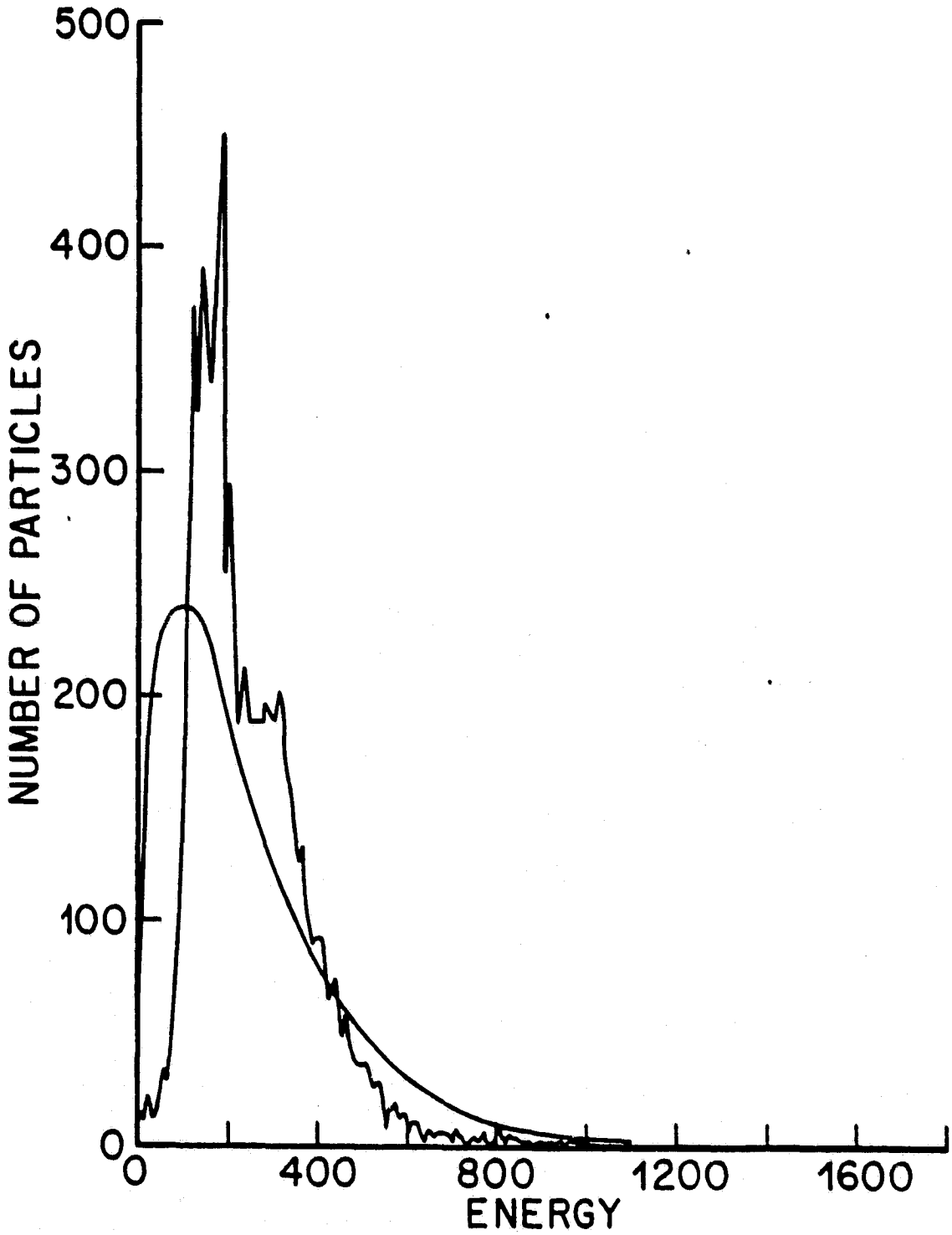

Figure 9. A plot showing the kinetic energy spectrum at the end of the run. The energy is in simulation units, $\frac{1}{2}v^2$. The smooth curve is the kinetic energy spectrum for a three-dimensional Maxwellian with the same number density and average energy.

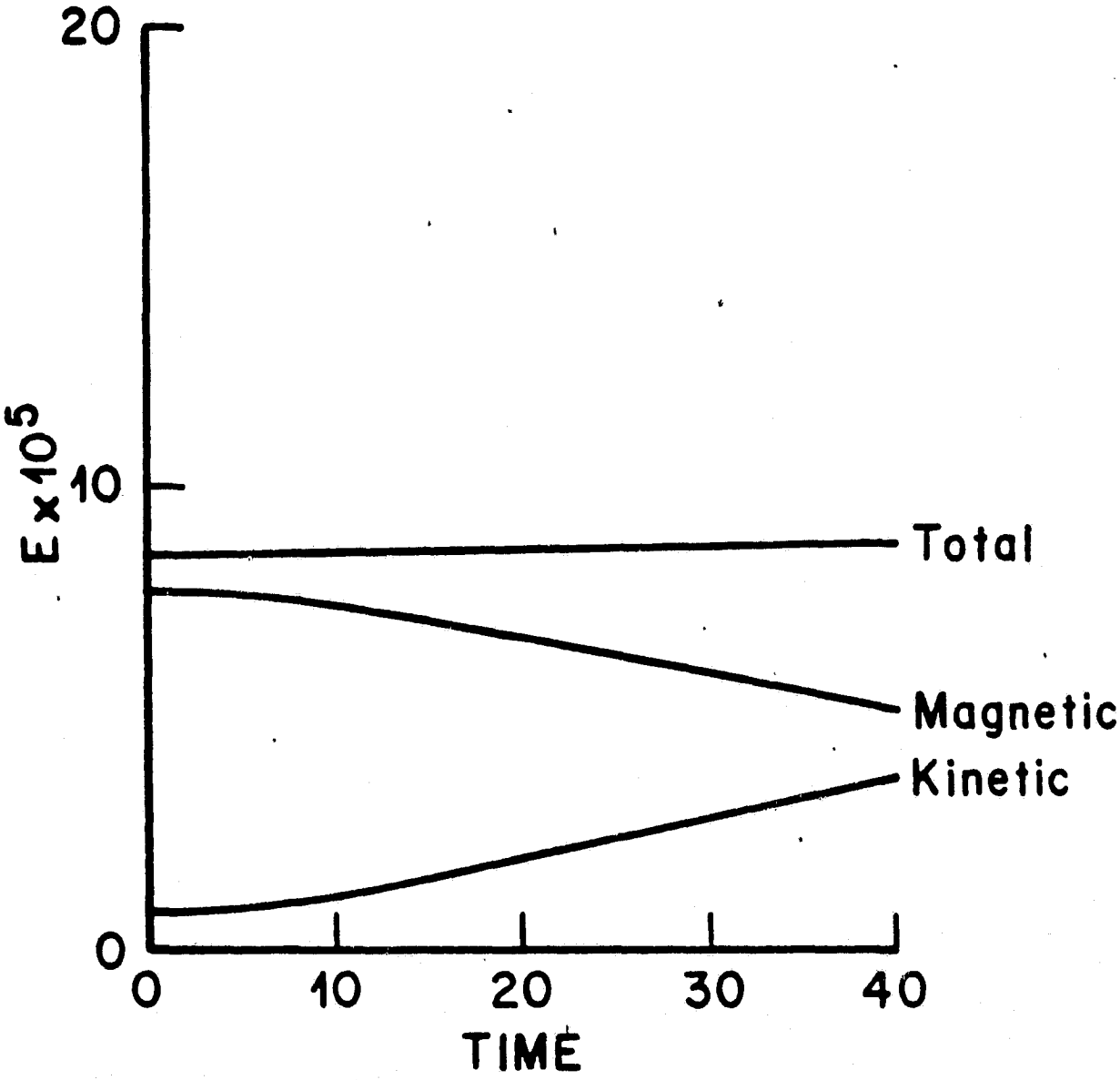

Figure 10. A plot showing the time variation of kinetic, magnetic and total energy during a run similar to that in Figure 8, except that the convection electric field was assumed to be zero.